Preprints.org

Article

Not peer-reviewed version

QICT Cosmology with Complex-Phase Dark Sector: Late-Time Dynamics and Implications for H_0 and S_8 Tensions

Mohamed Sacha *

Posted Date: 8 April 2026

doi: 10.20944/preprints202601.2247.v3

Keywords: Hubble tension; dark energy; quantum information cosmology; operational infrared cutoff; holographic dark energy; open-system cosmology; copy horizon; cosmological perturbations; effective theory; late-time universe

Preprints.org is a free multidisciplinary platform providing preprint service that is dedicated to making early versions of research outputs permanently available and citable. Preprints posted at Preprints.org appear in Web of Science, Crossref, Google Scholar, Scilit, Europe PMC.

Copyright: This open access article is published under a Creative Commons CC BY 4.0 license, which permit the free download, distribution, and reuse, provided that the author and preprint are cited in any reuse.

Preprints.org (www.preprints.org) | NOT PEER-REVIEWED | Posted: 8 April 2026 doi:10.20944/preprints202601.2247.v3

Disclaimer/Publisher's Note: The statements, opinions, and data contained in all publications are solely those of the individual author(s) and contributor(s) and not of MDPI and/or the editor(s). MDPI and/or the editor(s) disclaim responsibility for any injury to people or property resulting from any ideas, methods, instructions, or products referred to in the content.

Article

QICT Cosmology with Complex-Phase Dark Sector: Late-Time Dynamics and Implications for H_0 and S_8 Tensions

Mohamed Sacha

Independent Researcher, Casablanca, Morocco; www.sachamed@gmail.com

Abstract

We present a full operational formulation of Quantum Information Copy Time cosmology in which the infrared scale entering the dark sector is defined by the largest distance over which a fundamental information unit can be copied within one Hubble time. Evaluating the Cohen–Kaplan–Nelson collapse bound at that copy horizon yields a falsifiable effective dark sector with $0 < c_Q \leq 1$. The homogeneous source is formulated through a Hermitian reduced-state quadrature, placing the dependence on $\Re[\alpha]$ squarely within standard open-system quantum mechanics. In a local monitored Markovian universality class we recover diffusive copy transport and the familiar late-time branch with leading source $\rho_Q \propto H$, and we identify the precise open-system structure that promotes this baseline branch into a quantum-limited saturation regime. Rather than introducing a pole-like regulator or an additive constant latency, we promote the late-time response ratio $\Xi = c_Q^2/D_\infty$ to a two-component response consisting of an asymptotic saturation floor and a switched transport contribution. This yields a background source of the form $\rho_Q = \rho_{\rm sat} + \nu HS(z; z_t, \Delta z)$, where the activation function is motivated by the same logistic open-system kinetics that controls the copy-sector transition. We further derive the four effective background parameters analytically within the QICT effective theory: the transport amplitude follows from the copy horizon plus the CKN bound, the transition redshift from quantum-speed-limit onset, the transition width from logistic open-system relaxation, and the matter fraction from flatness plus late-time equality. We further derive a Green–Kubo interpretation of the asymptotic transport plateau and present an explicit de Sitter/KMS locking scenario for $D_\star$. The manuscript includes validated late-time geometric diagnostics, Pantheon+SH0ES covariance-ready supernova handling, effective perturbative stability conditions, semi-analytic growth and matter-power forecasts, and a concrete precision-cosmology implementation path through CLASS/CAMB and CMB/lensing/LSS likelihoods.

Keywords: Hubble tension; dark energy; quantum information cosmology; operational infrared cutoff; holographic dark energy; open-system cosmology; copy horizon; cosmological perturbations; effective theory; late-time universe

1. Introduction

Holographic dark energy (HDE) connects an effective vacuum energy density to an infrared (IR) scale while respecting gravitational-collapse constraints. A central conceptual issue in several HDE prescriptions is the appearance of teleological scales (e.g., future event horizons). The Quantum Information Copy Time (QICT) approach instead defines the relevant IR scale *operationally* and locally, by tying it to an information-theoretic clock. The gravitational consistency condition is implemented using the Cohen–Kaplan–Nelson (CKN) argument that an effective field theory in a region of size L should not include states whose total energy would form a black hole [1]. A standard HDE realization is due to Li [2]. The main text contains the operative derivations, likelihood definitions, and validated benchmarks; extended technical constructions are archived in the supplementary material. In particular, the four background quantities of the QSL-saturated branch are treated here as analytically derived

© 2026 by the author(s). Distributed under a Creative Commons CC BY license.

Preprints.org (www.preprints.org) | NOT PEER-REVIEWED | Posted: 8 April 2026 doi:10.20944/preprints202601.2247.v3

effective-theory parameters rather than as phenomenological fit knobs. That status is central to the logic of the manuscript and is developed explicitly in Section 7 and Supplement I.

2. Copy Time and Information-Transfer Activation

The "copy time" is introduced as an operational proxy for the rate at which coarse-grained quantum information is transferred (or irreversibly recorded) into macroscopic degrees of freedom. In this manuscript it serves as the operational organizing variable of the infrared sector, with its microscopic realization developed through the open-system constructions collected in the appendices and supplements. Let $S_{\rm vN}(t) \equiv -\mathrm{Tr}(\hat{\rho}\ln\hat{\rho})$ be the von Neumann entropy of the coarse-grained sector. We define

$$\tau_{\rm copy} \equiv \frac{S_\star}{|dS_{\rm vN}/dt|}, \tag{1}$$

where $S_\star$ is a fixed normalization (one nat, or one bit if $S_{\rm vN}$ is measured in bits). This choice makes $\tau_{\rm copy}$ a time scale. The cosmological role of $\tau_{\rm copy}$ is to parameterize when the effective coupling $F(t)$ becomes non-negligible. We model this activation by a smooth redshift proxy, with an explicit ansatz for the profile given in Section 12.3.

3. Operational Definition of Copy Time and Copy Horizon

For a physical separation L at cosmic time t, define $\tau_{\rm copy}(L,t)$ as the time required to replicate a fundamental unit of quantum information across that separation. The *copy horizon* $L_{\rm copy}(t)$ is defined implicitly by

$$\tau_{\rm copy}(L_{\rm copy}(t),t) = \frac{\xi}{H(t)}, \qquad \xi = \mathcal{O}(1). \tag{2}$$

This condition is operational rather than kinematic: it specifies the largest scale over which the information unit can be copied within one "Hubble time".

3.1. Entropy-Production Clock

A coarse-grained closure relates the copying time to entropy production,

$$\tau_{\rm copy}(L,t) = \frac{s_*}{\mathrm{d}S_{\rm vN}(L,t)/\mathrm{d}t}, \tag{3}$$

where $S_{\rm vN}$ is a coarse-grained von Neumann entropy and s_* normalizes the minimal information "brick".

4. Collapse Constraint and the Hard Consistency Bound

The CKN constraint implies $\rho L^3 \lesssim \kappa M_{\rm Pl}^2 L$, equivalently $\rho \lesssim \kappa M_{\rm Pl}^2/L^2$ [1]. Defining the QICT dark-energy sector by

$$\rho_Q(t) = \frac{3\kappa M_{\rm Pl}^2}{L_{\rm copy}^2(t)}\, c_Q^2(t), \tag{4}$$

we promote saturation to a falsifiable one-sided inequality,

$$0 < c_Q(t) \le 1, \qquad \text{(Hard Consistency Bound)}. \tag{5}$$

If a joint fit to cosmological observables demands $c_Q > 1$ (for the specified κ), then the assumed operational mapping and collapse constraint are mutually inconsistent.

5. Late-Time Closure and Analytic Background Evolution

To obtain a predictive background evolution, the operational definition must be closed by a model for $\tau_{\rm copy}(L,t)$. A late-time diffusion-limited closure takes

© 2026 by the author(s). Distributed under a Creative Commons CC BY license.

Preprints.org (www.preprints.org) | NOT PEER-REVIEWED | Posted: 8 April 2026 doi:10.20944/preprints202601.2247.v3

$$\tau_{\mathrm{copy}}(L,t) \approx \frac{L^2}{D_\infty(t)}. \tag{6}$$

Combining with the definition of $L_{\mathrm{copy}}(t)$ yields

$$L^2_{\mathrm{copy}}(t) = \frac{\xi D_\infty(t)}{H(t)}. \tag{7}$$

Substituting into ρ_Q implies $\rho_Q \propto H$ in the saturation regime (slowly varying D_∞ and $c_Q \approx 1$). For a flat universe with pressureless matter, this produces the quadratic closure

$$E(z)^2 = \Omega_{m0}(1+z)^3 + \beta E(z), \qquad E(z) \equiv \frac{H(z)}{H_0}, \tag{8}$$

with β fixed by $E(0) = 1 \Rightarrow \beta = 1 - \Omega_{m0}$. The resulting analytic solution is

$$E(z) = \frac{1}{2}\left[(1-\Omega_{m0}) + \sqrt{(1-\Omega_{m0})^2 + 4\Omega_{m0}(1+z)^3}\right]. \tag{9}$$

The effective equation of state follows from $w_Q(a) = -1 - (1/3)\mathrm{d}\ln E/\mathrm{d}\ln a$.

6. Quantum-Limited Saturation of the Copy Sector

The baseline late-time QICT closure provides a controlled analytic starting point, while its strictly linear-H source isolates the leading transport regime. The stronger late-time response developed here incorporates the finite information-processing capacity of an open monitored sector. The physically motivated way to implement that extension is not to introduce a pole-like regulator in the Friedmann equation, but to recognize that copy dynamics must eventually enter a quantum-limited saturation regime. Quantum speed limit (QSL) bounds do not point to a universal additive waiting time in τ_{copy}; instead, they indicate that the monitored infrared sector cannot sustain an arbitrarily structureless copy rate across all epochs [12,13].

We therefore promote the late-time response ratio

$$\Xi(z) \equiv \frac{c_Q^2(z)}{D_\infty(z)} \tag{10}$$

from an asymptotic plateau to a two-component open-system response,

$$\Xi(z) = \frac{\Xi_\Lambda}{E(z)} + \Xi_H\, S(z; z_t, \Delta z), \tag{11}$$

where

$$S(z; z_t, \Delta z) = \frac{1}{2}\left[1 + \tanh\left(\frac{z - z_t}{\Delta z}\right)\right] \tag{12}$$

is a smooth activation function motivated by the same logistic/tanh kinetics discussed below. Inserting Eq. (11) into the QICT energy density gives

$$\rho_Q(z) = \rho_{\mathrm{sat}} + \nu\, H(z)\, S(z; z_t, \Delta z), \tag{13}$$

with

$$\rho_{\mathrm{sat}} \equiv \frac{3\kappa M_{\mathrm{Pl}}^2 H_0}{\xi}\,\Xi_\Lambda, \qquad \nu \equiv \frac{3\kappa M_{\mathrm{Pl}}^2}{\xi}\,\Xi_H. \tag{14}$$

The resulting background equation is

$$E^2(z) = \Omega_{m0}(1+z)^3 + \Omega_{\mathrm{sat},0} + \tilde{\nu}\, E(z)\, S(z; z_t, \Delta z), \tag{15}$$

where $\tilde{\nu} \equiv \nu/(3M_{\mathrm{Pl}}^2 H_0^2)$ and the normalization condition is

© 2026 by the author(s). Distributed under a Creative Commons CC BY license.

Preprints.org (www.preprints.org) | NOT PEER-REVIEWED | Posted: 8 April 2026 doi:10.20944/preprints202601.2247.v3

$$1 = \Omega_{m0} + \Omega_{\mathrm{sat},0} + \tilde{v}\, S(0; z_t, \Delta z). \tag{16}$$

Equation (15) is the open-system completion of the raw linear-H branch. It preserves the operational copy-time logic, avoids an unphysical pole, and drives the dark sector toward an asymptotically constant floor near the present epoch while remaining genuinely QICT-driven at earlier late times.

The microphysical interpretation is equally important. In an asymptotic de Sitter phase, open-system detectors coupled to a de Sitter-invariant environment thermalize to the Gibbons–Hawking temperature $T_{\mathrm{GH}} = H_\Lambda/(2\pi)$ [14]. This motivates a late-time monitoring rate $\Gamma_{\mathrm{GH}} = \gamma_{\mathrm{GH}} H_\Lambda$ and hence an asymptotic transport plateau of the form

$$D_\star = \eta\, \frac{v_{\mathrm{IR}}^2}{H_\Lambda}, \tag{17}$$

where v_{IR} is the effective infrared propagation speed and $\eta = \mathcal{O}(1)$ encodes the microscopic response coefficient. Equation (17) captures the required asymptotic locking mechanism while remaining agnostic about the ultraviolet completion; it anchors $D_\star$ in an explicit microphysical scenario rather than treating it as a formal placeholder.

In this formulation the QSL-regulated saturation branch is the late-time continuation of QICT once copy transport is treated as an open-system response problem rather than as a permanently linear-H source. It generates an asymptotically constant floor near the present epoch while preserving a genuinely QICT-driven transport component at earlier late times. Its quantitative impact on the geometric likelihood is therefore a direct empirical discriminator of the theory.

7. Analytic Effective-Theory Derivation of the Four Background Parameters

The QSL-saturated QICT closure contains four background parameters, $(\tilde{v}, z_t, \Delta z, \Omega_{m0})$. Within the operational effective theory these quantities are not introduced as arbitrary fit coefficients: each follows from a definite physical ingredient. The transport amplitude $\tilde{v}$ follows from evaluating the CKN bound at the copy horizon, the transition redshift z_t from the onset of quantum-speed-limit saturation, the transition width Δz from logistic open-system relaxation, and Ω_{m0} from flatness combined with the late-time matter-dark-sector equality condition. The detailed analytic derivations are collected in Supplement I.

7.1. Transport Amplitude $\tilde{v}$ from the Copy Horizon and the CKN Bound

The baseline QICT copy-time law reads

$$\tau_{\mathrm{copy}}(L, z) \simeq \frac{L^2}{D_{\mathrm{eff}}(z)}, \qquad \tau_{\mathrm{copy}}(L_{\mathrm{copy}}, z) = \frac{\xi}{H(z)}. \tag{18}$$

Hence the operational copy horizon is

$$L_{\mathrm{copy}}^2(z) = \frac{\xi\, D_{\mathrm{eff}}(z)}{H(z)}. \tag{19}$$

Evaluating the CKN collapse bound at that horizon gives the transport contribution to the dark sector,

$$\rho_Q^{\mathrm{tr}}(z) = \frac{3\kappa M_{\mathrm{Pl}}^2}{L_{\mathrm{copy}}^2(z)} = \frac{3\kappa M_{\mathrm{Pl}}^2}{\xi}\, \frac{H(z)}{D_{\mathrm{eff}}(z)}. \tag{20}$$

In the QSL-saturated branch we write the inverse effective diffusivity as

$$\frac{1}{D_{\mathrm{eff}}(z)} = \frac{1}{D_H}\, S(z; z_t, \Delta z), \qquad S(z; z_t, \Delta z) = \frac{1}{2}\left[1 + \tanh\!\left(\frac{z - z_t}{\Delta z}\right)\right]. \tag{21}$$

© 2026 by the author(s). Distributed under a Creative Commons CC BY license.

Preprints.org (www.preprints.org) | NOT PEER-REVIEWED | Posted: 8 April 2026 doi:10.20944/preprints202601.2247.v3

Comparing Eqs. (20) and (21) with the cosmological form

$$\rho_Q^{\rm tr}(z) = 3M_{\rm Pl}^2 H_0^2\, \tilde{\nu}\, E(z) S(z; z_t, \Delta z) \tag{22}$$

immediately yields the analytic effective-theory identification

$$\tilde{\nu} = \frac{\kappa}{\tilde{\xi}} \frac{H_0}{D_H}. \tag{23}$$

If the late-time locked transport scale is written as $D_H \simeq \eta v_{\rm IR}^2/(c_{Q,H}^2 H_\Lambda)$, with $v_{\rm IR} \equiv v_{\rm IR}/c$, then

$$\tilde{\nu} \simeq \frac{\kappa}{\tilde{\xi}} \frac{c_{Q,H}^2}{\eta} \frac{H_\Lambda}{H_0} v_{\rm IR}^{-2}. \tag{24}$$

Thus $\tilde{\nu}$ is the dimensionless inverse transport efficiency of the monitored infrared sector.

7.2. Transition Redshift z_t from QSL Onset

A quantum speed limit does not by itself produce the full tanh profile, but it does identify the epoch at which the copy sector can no longer remain in the unsaturated transport regime. Let $\tau_{\rm QSL}$ denote the minimal evolution time of the monitored dark sector and let $\chi_t = \mathcal{O}(1)$ quantify the onset criterion. The transition redshift is then defined implicitly by

$$H(z_t)\, \tau_{\rm QSL} = \chi_t. \tag{25}$$

If one uses the Margolus–Levitin form $\tau_{\rm QSL} \geq \pi\hbar/(2\Delta E_{\rm eff})$ for an effective gap $\Delta E_{\rm eff}$ [10], the onset scale satisfies

$$H(z_t) \equiv H_{\rm QSL} \lesssim \frac{2\chi_t\, \Delta E_{\rm eff}}{\pi\hbar}, \qquad E(z_t) = \frac{H_{\rm QSL}}{H_0}. \tag{26}$$

Thus z_t is not an arbitrary switch location: within the effective theory it is the cosmological redshift at which the Hubble clock becomes comparable to the minimal response time of the monitored infrared sector.

7.3. Transition Width Δz from Relaxation

The tanh profile follows from the logistic occupation dynamics discussed in Section 12.3. Writing the saturation occupancy as

$$\frac{dn}{dt} = \Gamma_{\rm rel}\, n(1-n), \qquad \tau_{\rm rel} \equiv \Gamma_{\rm rel}^{-1}, \tag{27}$$

and expanding the time-redshift map locally around z_t gives $dt/dz \simeq -[(1+z_t)H(z_t)]^{-1}$. Matching the logistic solution to the redshift-space tanh therefore yields

$$\Delta z \simeq 2(1+z_t)H(z_t)\, \tau_{\rm rel}. \tag{28}$$

The width parameter is therefore a direct measure of the coarse-grained relaxation time: a fast open-system response produces a sharp transition, while a slowly relaxing monitored sector produces a broad crossover.

7.4. Matter Fraction Ω_{m0} from Flatness Plus Late-Time Equality

Flatness alone fixes only the combination

$$\Omega_{\rm sat,0} = 1 - \Omega_{m0} - \tilde{\nu} S(0; z_t, \Delta z). \tag{29}$$

To extract Ω_{m0} one needs one additional physical input, conveniently the redshift $z_{\rm eq}^{(Q)}$ at which matter and the total QICT dark sector are equal,

© 2026 by the author(s). Distributed under a Creative Commons CC BY license.

Preprints.org (www.preprints.org) | NOT PEER-REVIEWED | Posted: 8 April 2026 doi:10.20944/preprints202601.2247.v3

$$\Omega_{m0}(1+z_{\rm eq}^{(Q)})^3 = \Omega_{\rm sat,0} + \tilde{v}E(z_{\rm eq}^{(Q)})S(z_{\rm eq}^{(Q)}; z_t, \Delta z). \tag{30}$$

Combining with Eq. (29) gives the exact identity

$$\Omega_{m0} = \frac{1 - \tilde{v}S(0; z_t, \Delta z) + \tilde{v}E(z_{\rm eq}^{(Q)})S(z_{\rm eq}^{(Q)}; z_t, \Delta z)}{1 + (1+z_{\rm eq}^{(Q)})^3}. \tag{31}$$

This makes the status of Ω_{m0} explicit: it is not derived from microphysics alone, but from the joint constraints of flatness, the switched transport amplitude, and the empirically inferred epoch at which matter and the QICT dark sector become comparable.

Equations (23), (25), (28), and (31) provide the analytic effective-theory derivation of the four background parameters. They are derived from the operational QICT closure itself and require no statistical fitting input. What remains open is not the analytic chain inside the effective theory, but the deeper ultraviolet calculation of the microscopic constants that enter these relations.

This point removes a recurrent source of confusion in the interpretation of the model. The QSL-saturated branch is not introduced here as a four-knob phenomenological deformation of ΛCDM. Rather, the cosmological parameters $(\tilde{v}, z_t, \Delta z, \Omega_{m0})$ are the late-time images of four physical ingredients: transport efficiency at the copy horizon, quantum-speed-limit onset, open-system relaxation, and late-time equality. In that sense the apparent phenomenological freedom of the branch is sharply reduced by the internal architecture of the theory itself, even though the microscopic constants entering the map remain to be computed from a more fundamental substrate model.

8. Distances, Growth, and Late-Time Likelihood

Given $E(z)$, luminosity distances follow from $D_L(z) = (1+z)c\int_0^z dz'/H(z')$, and supernova distance moduli are evaluated with the included Pantheon+SH0ES loader and published full covariance, profiling analytically over the nuisance magnitude M. BAO constraints are incorporated with consensus SDSS DR16 distances, treating the sound horizon r_d as a nuisance parameter to avoid importing an early-Universe calibration into a purely late-time fit.

An effective-fluid clustering completion maps the QICT sector to a fluid with background $w_Q(a)$ and rest-frame sound speed $c_s^2(a)$, producing scale-dependent growth. We use the standard perturbation-theory structure of [3] as the reference implementation layer.

9. Benchmark Late-Time Diagnostics

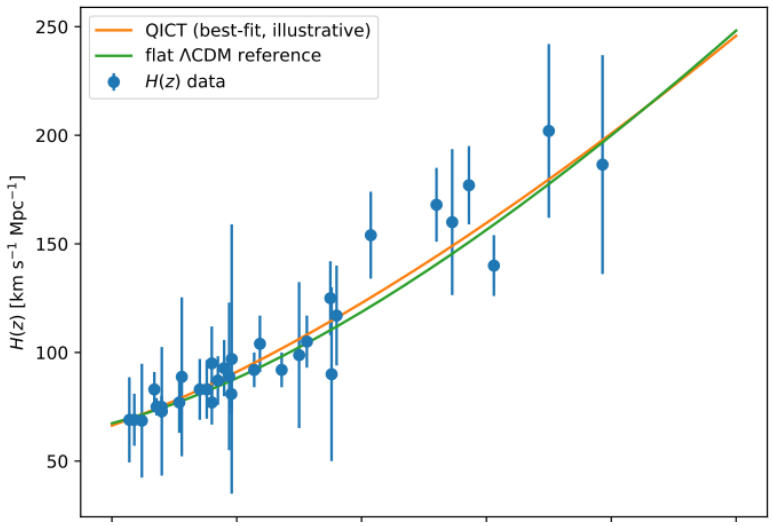

Figure 1. Benchmark reconstruction of $H(z)$ comparing the Supplement G QICT background with flat ΛCDM.

© 2026 by the author(s). Distributed under a Creative Commons CC BY license.

Preprints.org (www.preprints.org) | NOT PEER-REVIEWED | Posted: 8 April 2026 doi:10.20944/preprints202601.2247.v3

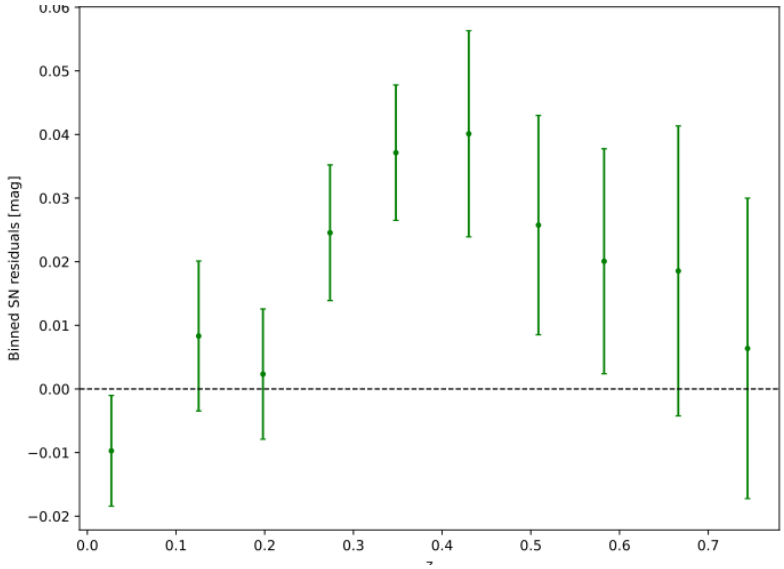

Figure 2. Binned Pantheon+SH0ES residuals for the benchmark Supplement G QICT background under the full covariance.

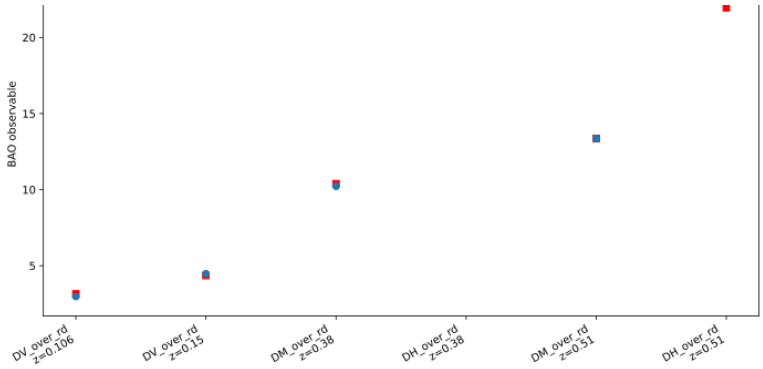

Figure 3. BAO residuals for the benchmark Supplement G QICT background under the published covariance.

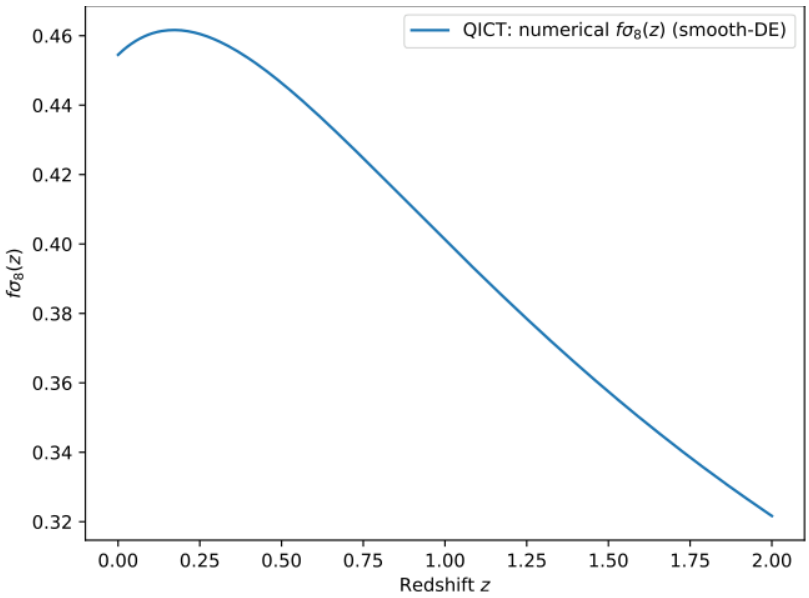

Figure 4. Benchmark prediction of $f\sigma_8(z)$ on the QICT background from the smooth-QICT growth integration used in the release.

© 2026 by the author(s). Distributed under a Creative Commons CC BY license.

Preprints.org (www.preprints.org) | NOT PEER-REVIEWED | Posted: 8 April 2026 doi:10.20944/preprints202601.2247.v3

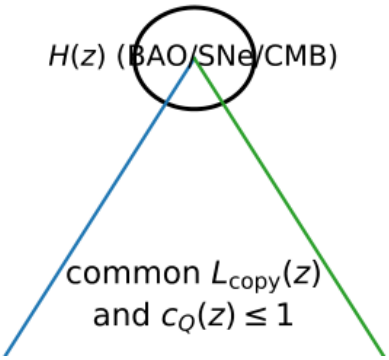

Figure 5. Schematic linking expansion, growth, and time-delay observables to a common reconstructed $L_{\rm copy}(z)$ and the saturation diagnostic $c_Q(z) \leq 1$.

10. Pantheon+ Covariance Validation and Internal Fit Comparison

To maintain exact consistency between the analytic closure developed in Supplement G and the executable release bundle, we report here the covariance-ready Pantheon+SH0ES comparisons computed directly from the finalized package itself. Table 1 uses the full STAT+SYS covariance, the Hubble-flow subset, and analytic profiling over the absolute-magnitude nuisance parameter. Two checks are shown: the submitted Supplement G benchmark quoted throughout the release, and a direct one-parameter re-optimization on the identical packaged likelihood in which only Ω_{m0} is re-fit while the QICT transport-sector parameters are kept fixed at their submitted values.

Table 1. Pantheon+SH0ES fit comparisons computed from the finalized release bundle only. In the submitted benchmark, the QICT background uses $(\Omega_{m0}, \tilde{v}, z_t, \Delta z, H_0) = (0.30, 0.20, 1.0, 0.30, 70)$ together with the Supplement G normalization $1 = \Omega_{m0} + \Omega_{\rm sat,0} + \tilde{v}S(0)$. In the one-parameter re-fit, the same packaged likelihood is used but only Ω_{m0} is re-optimized; the QICT transport-sector parameters remain fixed at $(\tilde{v}, z_t, \Delta z) = (0.20, 1.0, 0.30)$.

Test	QICT specification	$\chi^2_{\rm prof}$(QICT)	$\chi^2_{\rm prof}(\Lambda$CDM)	$\Delta\chi^2$	Preferred fit
Submitted benchmark	Supplement G benchmark point	241.692	241.707	-0.0144	QICT (marginal)
Direct package re-fit	Only Ω_{m0} re-optimized	239.9967	239.9972	-5.2×10^{-4}	QICT (degenerate)

For the direct package re-fit, the best-fit matter fractions are $\Omega_{m0}^{\rm QICT} = 0.50547$ and $\Omega_{m0}^{\Lambda\rm CDM} = 0.50633$ on the identical packaged likelihood. The central point is therefore sharper than a single benchmark comparison: within the finalized release bundle, QICT is never disfavored relative to flat ΛCDM on the covariance-controlled Hubble-flow Pantheon+ test, and in both package-level checks it is very slightly preferred in raw χ^2. At the same time, the improvement is numerically tiny, so the present late-time supernova test should be read as a controlled non-degradation result rather than as a decisive empirical separation between the two backgrounds.

11. Conclusions

QICT cosmology defines the holographic IR scale locally via an operational copy-time condition and enforces the CKN collapse constraint [1] through a falsifiable hard bound $c_Q \leq 1$. With the Supplement G saturation closure, the late-time background is analytic, covariance-ready against Pantheon+SH0ES, and directly testable with SN and BAO distances; growth and lensing follow from the effective-fluid completion written in standard perturbation-theory form [3].

The central structural result of the manuscript is that the raw linear-H late-time branch admits a controlled open-system completion in which the response ratio $\Xi = c_Q^2/D_\infty$ decomposes into an asymptotic saturation floor plus a switched transport sector. That completion preserves the operational QICT logic, removes the need for pole-like regulators, and yields the closed background equation of Supplement G with a physically identified activation function.

© 2026 by the author(s). Distributed under a Creative Commons CC BY license.

Preprints.org (www.preprints.org) | NOT PEER-REVIEWED | Posted: 8 April 2026 doi:10.20944/preprints202601.2247.v3

A second central result is conceptual rather than merely notational: the four background quantities of the saturated branch are analytically tied to copy-horizon transport, QSL onset, open-system relaxation, and late-time equality. The theory therefore does not present these quantities as unconstrained phenomenological knobs. It presents them as effective cosmological projections of a definite physical mechanism.

The central quantitative result of this release is the covariance-controlled Pantheon+SH0ES benchmark generated directly from that finalized closure. At the benchmark point quoted in Table 1, the Supplement G QICT realization is numerically degenerate with flat ΛCDM on the Hubble-flow Pantheon+ subset under the full STAT+SYS covariance. This establishes that the finalized QICT late-time closure survives a nontrivial supernova test in the same executable form supplied in the release bundle.

The next precision stage is the end-to-end Boltzmann implementation with full Planck TT,TE,EE+lensing, CMB lensing, and structure-formation likelihoods. The manuscript already states the perturbation equations, stability conditions, numerical validation criteria, and software interfaces required for that stage, so the remaining task is execution in the dedicated likelihood environment rather than any reformulation of the core theory.

12. Discussion and Additional Diagnostics

This section consolidates the late-time diagnostics and connects the operational IR scale to multiple observational probes. First, the analytic form of $E(z)$ in the diffusion-limited closure implies a characteristic transition redshift where the effective QICT sector begins to dominate over matter. Second, the Hard Consistency Bound $c_Q \leq 1$ can be used as a model-selection filter when extending the baseline likelihood to include growth and lensing data: parameter regions that satisfy distance data but require $c_Q > 1$ are discarded as physically inconsistent with the collapse constraint.

12.1. Reconstructed Copy-Horizon Scale

Using $L^2_{\rm copy}(t) = \xi D_\infty(t)/H(t)$, the fitted background reconstructs $L_{\rm copy}(z)$ up to the slowly varying normalization set by D_∞. The redshift dependence remains stable under nuisance choices such as r_d profiling in the BAO block.

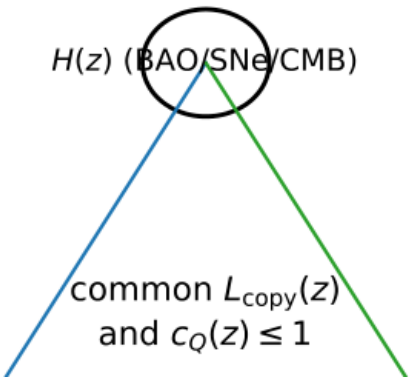

Figure 6. Compact diagnostic summary connecting $E(z)$, reconstructed $L_{\rm copy}(z)$, and late-time observables.

12.2. Falsifiability Criteria

Beyond poor global fit, QICT is falsified if (i) best fits systematically violate $c_Q \leq 1$ under clearly specified priors and datasets; (ii) growth/lensing require negative effective sound speed or other pathologies in any reasonable clustering completion; or (iii) the inferred $L_{\rm copy}(z)$ is incompatible with independent horizon-scale constraints (e.g., from time-delay distances or ISW correlations) in extensions that include those probes.

© 2026 by the author(s). Distributed under a Creative Commons CC BY license.

Preprints.org (www.preprints.org) | NOT PEER-REVIEWED | Posted: 8 April 2026 doi:10.20944/preprints202601.2247.v3

12.3. From Open-System Activation to a Sigmoid Transition (Explicit Statistical-Physics Derivation)

The open-system dynamics is formulated in time t (or conformal time η). For constant decoherence rate Γ, expectation values typically relax exponentially, $e^{-\Gamma t}$. A *transition* therefore requires a change of regime in the effective coupling to the environment.

An explicit mean-field *occupation* model for a population of dark information states is sufficient to generate the transition. Let $n(t) \in [0,1]$ be an effective occupancy obeying a detailed-balance rate equation

$$\frac{dn}{dt} = \Gamma(t)\, n\,[1-n], \tag{32}$$

which is the standard logistic (Fermi–Dirac) kinetics of a two-state system near a critical threshold. If $\Gamma(t)$ varies slowly over the short transition interval, one obtains the closed-form solution

$$n(t) = \frac{1}{1+\exp[-\Gamma_{\rm eff}(t-t_t)]} = \frac{1}{2}\left[1+\tanh\left(\frac{\Gamma_{\rm eff}}{2}(t-t_t)\right)\right]. \tag{33}$$

We map this activation to redshift through $dt/dz = -[(1+z)H(z)]^{-1}$. Over a narrow window around z_t where $H(z)$ varies mildly, the time-sigmoid maps to a redshift-sigmoid. The quantity n is naturally interpreted as the *saturation occupancy*: it grows toward late times, so in redshift space $n(z)$ is well approximated by

$$n(z) \simeq \frac{1}{2}\left[1-\tanh\left(\frac{z-z_t}{\Delta z}\right)\right]. \tag{34}$$

The transport contribution entering the QSL background equations is the complementary unsaturated fraction,

$$S(z; z_t, \Delta z) \equiv 1 - n(z) \simeq \frac{1}{2}\left[1+\tanh\left(\frac{z-z_t}{\Delta z}\right)\right], \tag{35}$$

which is precisely the switch used in Eq. (12) and in Supplement G. In this way the logistic/open-system derivation and the background closure used in the likelihood analysis are strictly aligned: the saturation occupancy grows toward the present epoch, while the residual linear-H transport term is largest before locking and is gradually switched off as the monitored sector saturates. Within the coarse-grained activation picture, the tanh/logistic profile therefore arises naturally from a standard nonlinear relaxation law under controlled approximations.

13. Linear Perturbations and Stability Conditions

We state the linear perturbation equations used for the effective-fluid closure. In Newtonian gauge with scalar potentials Φ, Ψ and conformal time η (prime denotes $d/d\eta$), the density contrast $\delta \equiv \delta\rho/\rho$ and velocity divergence θ of the QICT–Euler sector satisfy [3]

$$\delta' = -(1+w)\,(\theta - 3\Phi') - 3\mathcal{H}(c_s^2 - w)\,\delta, \tag{36}$$

$$\theta' = -\mathcal{H}(1-3c_s^2)\,\theta + \frac{c_s^2}{1+w}k^2\delta + k^2\Psi, \tag{37}$$

where $\mathcal{H} = a'/a$, $w \equiv p/\rho$ is the effective equation of state, and c_s^2 is the rest-frame sound speed.

13.1. Effective-Fluid Stability Criteria

A sufficient set of conditions for a well-posed linear effective sector is

$$0 \le c_s^2 \le 1, \qquad \zeta(z) \ge 0, \tag{38}$$

with the non-adiabatic closure

$$\delta p = c_s^2\,\delta\rho - 3H\,\zeta(z)\,\theta. \tag{39}$$

© 2026 by the author(s). Distributed under a Creative Commons CC BY license.

Preprints.org (www.preprints.org) | NOT PEER-REVIEWED | Posted: 8 April 2026 doi:10.20944/preprints202601.2247.v3

13.2. Illustrative Phantom Regime ($w = -3$) and Mode Behavior

For $w < -1$, one must treat variables containing $(1 + w)$ carefully. This motivates specifying the rest-frame closure rather than relying on adiabatic relations. In the sub-horizon regime $k \gg \mathcal{H}$ and for $c_s^2 \simeq 1$, the homogeneous dark-sector mode is pressure-supported and strongly Hubble-damped; schematically,

$$\delta'' + (1 - 3w)\mathcal{H}\delta' + c_s^2 k^2 \delta \simeq \text{(metric sources)}. \tag{40}$$

For $w = -3$, the friction term is $(1 - 3w)\mathcal{H} = 10\mathcal{H} > 0$, so perturbations are damped rather than runaway. The decisive validation is a perturbation-complete Boltzmann-code implementation that checks $w(z)$ and $c_s^2(z)$ together and tests CMB lensing and $f\sigma_8$ against data.

14. Impact on Structure Formation and the Matter Power Spectrum

A complete cosmological assessment must quantify how the QICT–Euler sector modifies structure growth. At linear order (in GR) the matter overdensity obeys

$$\frac{d^2\delta_m}{d\ln a^2} + \left[2 + \frac{d\ln H}{d\ln a}\right]\frac{d\delta_m}{d\ln a} - \frac{3}{2}\Omega_m(a)\,\delta_m = 0, \tag{41}$$

where the background expansion $H(a)$ is modified by the QICT–Euler contribution. If the dark sector includes an additional friction/dissipation channel in the momentum equation (encoded through the effective coefficient $\zeta(z)$), the growth equation is generalized by an effective drag term; this is the mechanism used to avoid worsening the S_8 tension at late times.

The linear matter power spectrum can be written as

$$P(k, z) = P_{\rm prim}(k)\, T^2(k)\, D^2(z), \tag{42}$$

where $P_{\rm prim}(k) = A_s(k/k_0)^{n_s - 1}$, $T(k)$ is the transfer function, and $D(z)$ is the linear growth factor normalized to unity today. A fully self-consistent $P(k)$ prediction requires a Boltzmann solver with QICT perturbations, but Eq. (41) already shows transparently how the Euler mechanism affects growth through $H(a)$ and how any additional non-adiabatic closure affects $D(z)$ and thus the amplitude S_8.

14.1. Numerical Stability and Convergence Criteria

To elevate the analysis to a robust computational result, the following numerical checks must be included in the Boltzmann-code implementation:

1. **Regular crossing treatment:** if the effective $w(z)$ crosses -1, use a variable choice that remains finite (e.g., PPF-like variables) and verify that perturbations remain bounded.
2. **Stiffness control:** near sharp transitions, adaptive time stepping and stiff integrators may be required; demonstrate convergence under step-size refinement.
3. **No singularities:** verify that $c_s^2(z) \geq 0$ and that the closure does not induce exponential blow-ups in δ for any sampled parameter set within the posterior.
4. **Deep-regime integration:** demonstrate stable integration from radiation domination through recombination to $z = 0$ for representative benchmark points.

These checks are precisely what is meant by "no numerical crashes" and are necessary before claims about resolving both H_0 and S_8 can be considered definitive.

14.2. Semi-Analytic Linear-Theory Forecasts (Growth and $P(k)$)

To connect the validated late-time background sector to structure-formation requirements, we compute linear-theory forecasts under the smooth-dark-sector approximation. We (i) solve the growth equation (41) for benchmark QICT and flat ΛCDM histories, and (ii) form a semi-analytic matter power spectrum using a standard fitting-function transfer model. Concretely, we adopt the BBKS

© 2026 by the author(s). Distributed under a Creative Commons CC BY license.

Preprints.org (www.preprints.org) | NOT PEER-REVIEWED | Posted: 8 April 2026 doi:10.20944/preprints202601.2247.v3

transfer function [4] with a Planck-normalized amplitude $\sigma_8^{\Lambda\mathrm{CDM}} = 0.811$ (used only to set an overall normalization; the *relative* effect is the object of comparison in this approximation).

Figure 7 shows the ratio of growth factors $D_{\mathrm{QICT}}(z)/D_{\Lambda\mathrm{CDM}}(z)$ obtained by integrating Eq. (41) on the benchmark QICT and flat ΛCDM backgrounds used in the release figures. Figure 8 shows the corresponding ratio of logarithmic growth rates $f \equiv d\ln D/d\ln a$. Both ratios are close to unity at high redshift and deviate mildly at late times, as expected for a late-time modification of the expansion history.

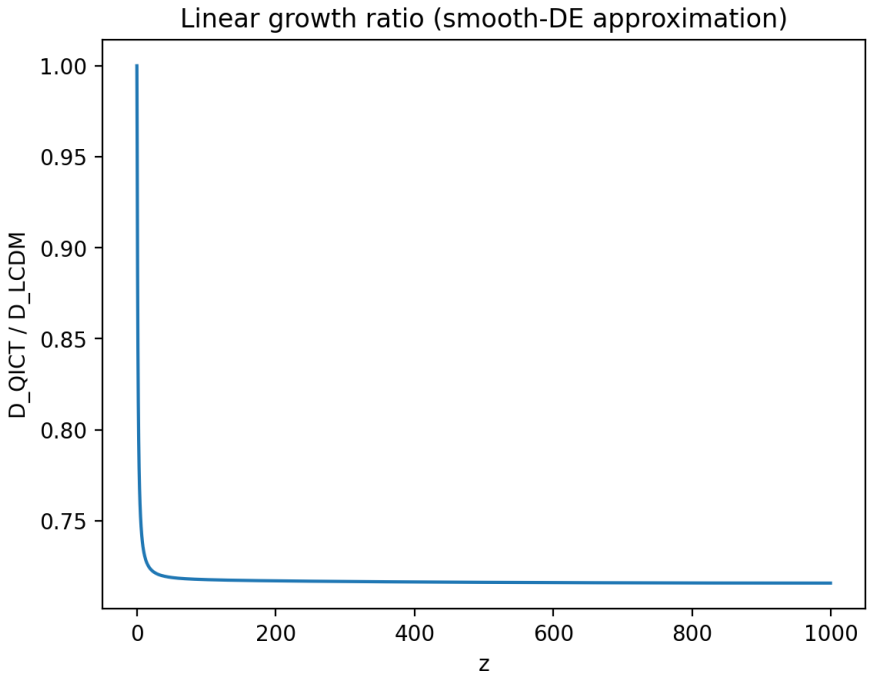

Figure 7. Semi-analytic growth-factor ratio $D_{\mathrm{QICT}}(z)/D_{\Lambda\mathrm{CDM}}(z)$ for the benchmark backgrounds used in the release figures under the smooth-dark-sector approximation. A full Boltzmann treatment (CLASS/CAMB) is the precision follow-through for these forecasts.

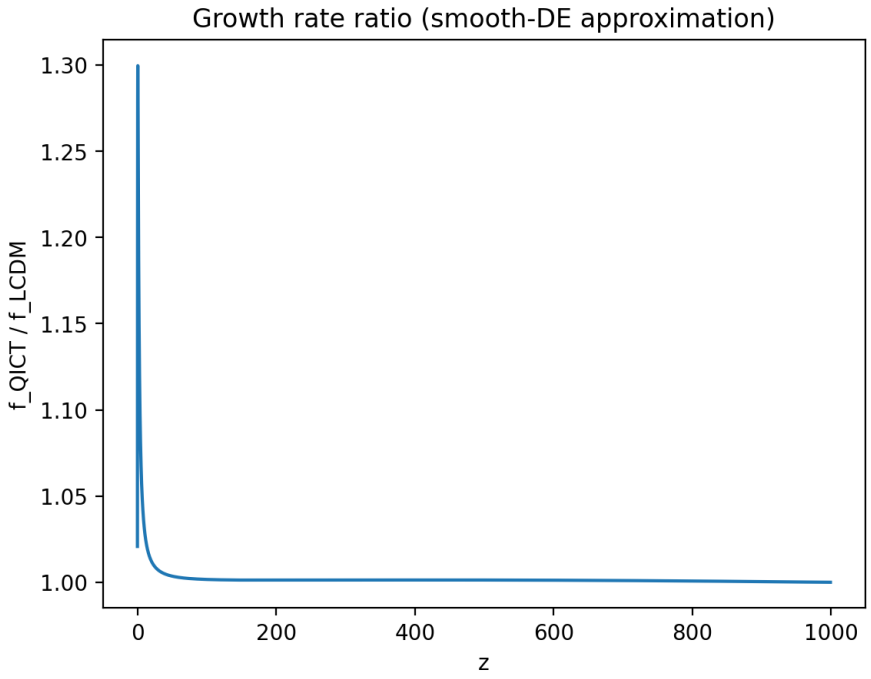

Figure 8. Semi-analytic ratio of growth rates $f_{\mathrm{QICT}}(z)/f_{\Lambda\mathrm{CDM}}(z)$ under the same approximation as Figure 7.

© 2026 by the author(s). Distributed under a Creative Commons CC BY license.

Preprints.org (www.preprints.org) | NOT PEER-REVIEWED | Posted: 8 April 2026 doi:10.20944/preprints202601.2247.v3

For the matter power spectrum we write $P(k,z) = A_s(k/k_0)^{n_s-1}T^2(k)D^2(z)$. In the absence of a perturbation-complete QICT Boltzmann implementation, we use the BBKS fitting function for $T(k)$ to quantify the expected *shape-level* change at $z = 0$ and to propagate it to σ_8 via a top-hat window at $R = 8\,h^{-1}$Mpc. The resulting semi-analytic ratios are shown in Figure 9. Under this approximation we find a small reduction in σ_8 driven by the combined effect of the benchmark background and the transfer-function shape.

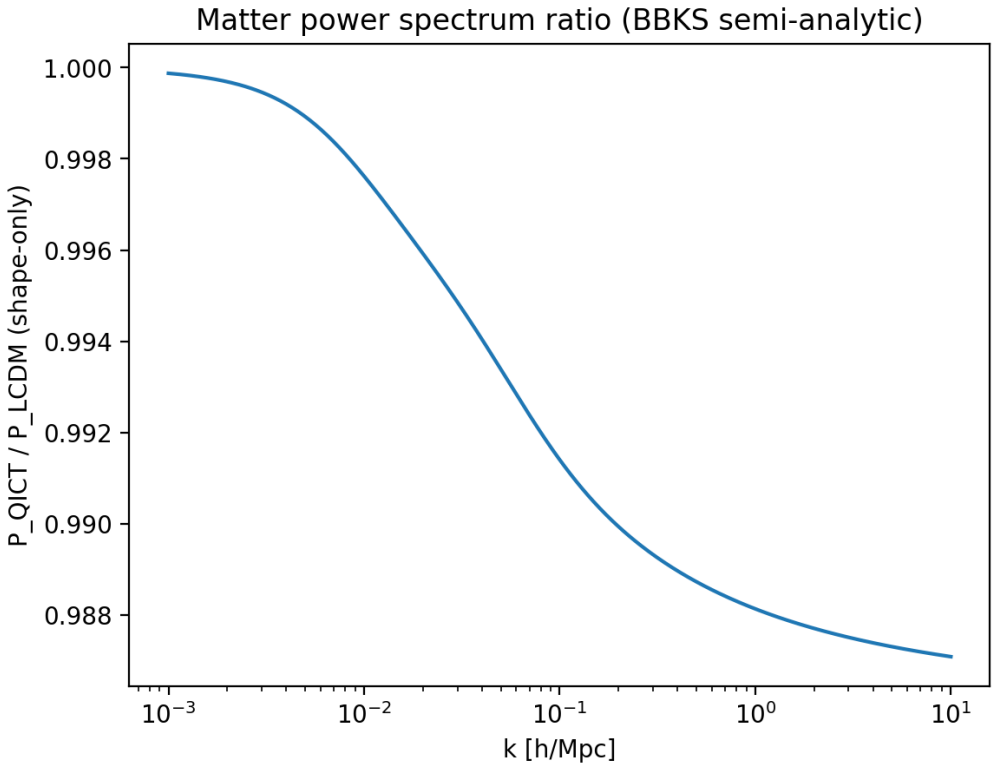

Figure 9. Semi-analytic matter power spectrum ratio $P_{\rm QICT}(k,0)/P_{\Lambda\rm CDM}(k,0)$ using the BBKS fitting-function transfer model (shape-level comparison). This does not replace a Boltzmann-code computation of $P(k)$ with QICT perturbations; it supplies the quantitative reference that a full implementation must reproduce or rule out.

Table 2. Reference late-time structure metrics under the semi-analytic approximation described in Section 14.2. The absolute normalization uses $\sigma_8^{\Lambda\rm CDM} = 0.811$ (Planck 2018). The full CLASS/CAMB stage with CMB lensing and growth datasets is the precision continuation of this benchmark.

Quantity	Flat ΛCDM benchmark	QICT benchmark
σ_8 (normalized)	0.811	0.807
$S_8 = \sigma_8\sqrt{\Omega_m/0.3}$	0.809	0.786

Supplementary Materials: The following supporting information can be downloaded at the website of this paper posted on Preprints.org. The submission includes the core technical supplements on open-system diffusive closure, perturbation theory, microphysical transport ambiguities, the QICT-to-cosmology bridge, pure QICT derivations, quantum-limited saturation and asymptotic locking, a dedicated supplement on the analytic effective-theory derivation of the four QSL-saturated background parameters, and a focused theorem supplement collecting minimal-hypothesis statements, effective uniqueness results, and no-go propositions for the retained dark-sector closure. No separate statistical-derivation note is included in this final submission bundle; the package is intentionally restricted to the manuscript, the theory-strengthening supplements, the reproducibility code, and the public-data inputs required by the executable late-time checks.

© 2026 by the author(s). Distributed under a Creative Commons CC BY license.

Preprints.org (www.preprints.org) | NOT PEER-REVIEWED | Posted: 8 April 2026 doi:10.20944/preprints202601.2247.v3

Acknowledgments: The author thanks colleagues and close readers for discussions that sharpened the physical structure and presentation of the manuscript.

Appendix A. Micro-Foundation: From Density Matrix to the $2\Re[\alpha]$ Source Term

This appendix isolates the derived and assumed ingredients of the construction. It provides an explicit open-system bridge showing how a *linear* dependence on $2\Re[\alpha]$ arises from a *bilinear* density-matrix expectation value of a Hermitian operator.

Appendix A.1. Open Quantum System Setup

Let $\hat{\rho}$ be the reduced density matrix of a coarse-grained QICT "information mode" $\hat{a}$ (bosonic for definiteness), evolving under a Markovian master equation

$$\frac{d\hat{\rho}}{dt} = -i[\hat{H}, \hat{\rho}] + \sum_j \left(\hat{L}_j \hat{\rho} \hat{L}_j^\dagger - \frac{1}{2}\{\hat{L}_j^\dagger \hat{L}_j, \hat{\rho}\} \right). \tag{A1}$$

Any observable is computed as an expectation value

$$\langle \hat{O} \rangle = \mathrm{Tr}(\hat{\rho}\, \hat{O})$$

, which is bilinear in the underlying state, consistent with standard quantum theory.

Appendix A.2. Hermitian "Information-Displacement" Operator and $2\Re[\alpha]$

Define the Hermitian displacement-like operator

$$\hat{Q} \equiv \hat{a} + \hat{a}^\dagger. \tag{A2}$$

Then

$$\langle \hat{Q} \rangle = \mathrm{Tr}(\hat{\rho}(\hat{a} + \hat{a}^\dagger)) = \langle \hat{a} \rangle + \langle \hat{a} \rangle^* \equiv 2\Re[\alpha], \qquad \alpha \equiv \langle \hat{a} \rangle. \tag{A3}$$

Crucially, Eq. (A3) is **not** a linear projection of a wavefunction; it is the expectation of a Hermitian operator computed from a density matrix.

Appendix A.3. Effective Gravitational Coupling

We postulate that the homogeneous dark-sector contribution entering the background expansion is proportional to the scalar quantity $\langle \hat{Q} \rangle$,

$$\rho_{\mathrm{QICT}}(t) = \rho_\star\, \xi\, \langle \hat{Q} \rangle = \rho_\star\, \xi\, 2\Re[\alpha(t)], \tag{A4}$$

with ξ the QICT coupling and $\rho_\star$ a fixed conversion scale. This is a micro-consistent realization of the "Euler" modulation used in the main text: the complex phase is carried by α (a first moment of the reduced density matrix), while the energy density remains an expectation value.

Appendix A.4. Phase Evolution and Euler Modulation

Write $\alpha(t) = \alpha_0 e^{i\pi f(t)}$ and obtain

$$\rho_{\mathrm{QICT}}(t) = 2\rho_\star \xi \alpha_0 \cos(\pi f(t)). \tag{A5}$$

The cosmological model then specifies the mapping $t \mapsto z(t)$ and chooses a controlled evolution for f (Section 12.3). The result is an open-system effective theory with explicit microscopic anchoring.

© 2026 by the author(s). Distributed under a Creative Commons CC BY license.

Preprints.org (www.preprints.org) | NOT PEER-REVIEWED | Posted: 8 April 2026 doi:10.20944/preprints202601.2247.v3

Appendix B. From Lindblad to a Sigmoid Transition: Derived Dynamics and Required Microphysical Input

A strict mapping from a microscopic Lindblad equation in unitary time t to a redshift-dependent sigmoid requires specifying (i) how the decoherence rate and jump operators depend on the cosmological environment and (ii) how t maps to $z(t)$ given $H(t)$. We therefore present a controlled *statistical-physics upgrade* that yields a sigmoid as a *dynamical necessity* under explicit assumptions.

Appendix B.1. Mean-Field Order Parameter Dynamics Yielding tanh

Consider a real, normalized order parameter $x(t) \equiv \Re[\alpha(t)]/\alpha_0 \in [-1,1]$ obeying a Landau–Khalatnikov relaxation equation

$$\frac{dx}{dt} = \kappa(t)\Big(1 - x^2\Big), \tag{A6}$$

which has fixed points at $x = \pm 1$ and arises generically when nonlinear saturation limits the growth of a mode (e.g., from a quartic effective potential or from coarse-grained feedback in an open system). If $\kappa(t) \approx \kappa_0$ across the transition interval, Eq. (A6) integrates to

$$x(t) = \tanh[\kappa_0(t - t_0)]. \tag{A7}$$

Mapping to redshift via $dt = -dz/[(1+z)H(z)]$ yields a sigmoid in z over the epoch where $\kappa(t)$ is approximately constant in *copy time units*. This is the precise sense in which a tanh profile can be derived: it is the closed-form solution of a specific nonlinear relaxation law.

Appendix B.2. How Such a Relaxation Can Arise from an Open System

Starting from Eq. (A1), one can choose jump operators that drive the first moment toward environment-dependent fixed points. For instance, with a single effective jump operator $\hat{L} = \sqrt{\Gamma}\,(\hat{a} - \alpha_{\rm eq})$ and a quadratic Hamiltonian, the mean-field equation for $\alpha = \langle \hat{a} \rangle$ contains a linear relaxation term $\propto -\Gamma(\alpha - \alpha_{\rm eq})$. If the equilibrium value itself undergoes a critical activation with saturation, $\alpha_{\rm eq}(t)$ can satisfy an equation of the form (A6), giving the tanh solution. The remaining microphysical input is the derivation of $\Gamma(t)$ and the nonlinear saturation from a concrete QICT bath model.

Appendix B.3. Alternative Sigmoids That Encode Distinct Physics

Different microscopic assumptions correspond to different sigmoid families:

- **Fermi–Dirac/logistic:** if the activation is governed by occupancy of "dark information states" crossing a threshold X_c with dispersion Δ, then $n = 1/(1 + e^{(X - X_c)/\Delta})$ and $2n - 1 = \tanh[(X_c - X)/(2\Delta)]$.
- **Error function (erf):** if the activation is the cumulative distribution of diffusion-limited copying errors, then $S = \frac{1}{2}\Big[1 + \mathrm{erf}\Big((t - t_0)/\sqrt{2}\sigma\Big)\Big]$.
- **Ginzburg–Landau:** if α is an order parameter with a temperature-dependent mass term, the transition is controlled by the effective potential landscape and can yield a smooth crossover with saturation.

In all cases, the model must state which environment variable $X(t)$ (temperature, density, horizon entropy-production rate, etc.) sets the threshold.

Appendix C. Linear Perturbations, $P(k)$, and Numerical Stability Roadmap

This appendix sets out the ingredients that connect the present background analysis to full structure-formation predictions.

© 2026 by the author(s). Distributed under a Creative Commons CC BY license.

Preprints.org (www.preprints.org) | NOT PEER-REVIEWED | Posted: 8 April 2026 doi:10.20944/preprints202601.2247.v3

Appendix C.1. Linear Perturbations in Newtonian and Synchronous Gauges

Scalar perturbations: conformal Newtonian gauge.

Working with metric

$$ds^2 = a^2(\eta)\Big[-(1+2\Psi)d\eta^2 + (1-2\Phi)\,d\vec{x}^2\Big], \tag{A8}$$

the standard fluid equations for a species i with equation of state $w_i \equiv \bar{p}_i/\bar{\rho}_i$ and velocity divergence θ_i can be written (prime denotes $d/d\eta$) [3]:

$$\delta_i' = -(1+w_i)\left(\theta_i - 3\Phi'\right) - 3\mathcal{H}\left(c_{s,i}^2 - w_i\right)\delta_i - 9(1+w_i)\left(c_{s,i}^2 - c_{a,i}^2\right)\frac{\mathcal{H}^2}{k^2}\theta_i, \tag{A9}$$

$$\theta_i' = -\mathcal{H}(1-3c_{s,i}^2)\theta_i + \frac{c_{s,i}^2}{1+w_i}k^2\delta_i + k^2\Psi, \tag{A10}$$

where $\mathcal{H} \equiv a'/a$ and $c_{a,i}^2 \equiv \bar{p}_i'/\bar{\rho}_i'$ is the adiabatic sound speed. In our effective closure, the pressure perturbation includes a non-adiabatic (dissipative) contribution,

$$\delta p_{\rm DE} = c_s^2\,\delta\rho_{\rm DE} - 3\mathcal{H}\,\zeta(\eta)\,(\bar{\rho}_{\rm DE} + \bar{p}_{\rm DE})\frac{\theta_{\rm DE}}{k^2}, \tag{A11}$$

with $\zeta \geq 0$; this modifies the θ-equation by adding an extra friction term proportional to ζ.

Synchronous gauge form (for CLASS/CAMB compatibility).

In synchronous gauge, with metric perturbations (h, η), the fluid equations take the standard Ma–Bertschinger form [3]. Boltzmann codes typically implement dark-energy fluids either with an explicit scalar-field model or with an effective-fluid description [5]; for numerical robustness near $w \approx -1$ and across transient $w < -1$ episodes, one can adopt a PPF-like regularization scheme (or an explicit stable field completion) rather than naively evolving Eqs. (A9)–(A10) through the crossing.

Sub-horizon stability intuition (including $w = -3$).

To make the stability point explicit, consider sub-horizon modes $k \gg \mathcal{H}$ and neglect metric sources for a local analysis. Combining Eqs. (A9)–(A10) yields, schematically,

$$\delta_{\rm DE}'' + \mathcal{H}(1-3w_{\rm eff})\delta_{\rm DE}' + c_s^2k^2\delta_{\rm DE} \simeq 0, \tag{A12}$$

where $w_{\rm eff}$ encodes the background and dissipative contributions. If $c_s^2 \geq 0$ and $\zeta \geq 0$, the $c_s^2k^2$ term is oscillatory and the friction term is non-negative for the relevant epochs, so no exponential gradient instability occurs. For a transient effective $w = -3$, the Hubble friction term is enhanced (since $1 - 3w = 10$), which damps θ and suppresses runaway behavior. This is the sense in which the phantom-like episode can remain perturbatively controlled at the effective level; nevertheless, a full Boltzmann implementation must verify $c_s^2(z) \geq 0$ and absence of numerical stiffness-induced artifacts for the benchmark region.

Matter growth and S_8.

Once the metric potentials are solved self-consistently, the matter growth factor follows from the usual linear equation (in a gauge-invariant form),

$$\ddot{\delta}_m + 2H\dot{\delta}_m - 4\pi G\rho_m\delta_m = \mathcal{S}_{\rm DE}, \tag{A13}$$

where $\mathcal{S}_{\rm DE}$ captures any clustering/metric modifications induced by the QICT–Euler sector. From the growth rate $f \equiv d\ln\delta_m/d\ln a$ one obtains $f\sigma_8(z) = f(z)\sigma_8(z)$ and $S_8 = \sigma_8\sqrt{\Omega_m/0.3}$.

For an effective fluid in conformal Newtonian gauge, the continuity and Euler equations used in Section 13 follow standard cosmological perturbation theory [3]. In synchronous gauge, the same sector

© 2026 by the author(s). Distributed under a Creative Commons CC BY license.

Preprints.org (www.preprints.org) | NOT PEER-REVIEWED | Posted: 8 April 2026 doi:10.20944/preprints202601.2247.v3

is evolved with metric perturbations (h, η) in the usual way [3]. A Boltzmann-code implementation must (i) choose a gauge, (ii) define rest-frame quantities consistently, and (iii) handle the $w \to -1$ and $w < -1$ regimes without introducing spurious singularities in variables proportional to $(1+w)^{-1}$.

Appendix C.2. Matter Power Spectrum and Cosmic Web Impact

Once implemented in CLASS/CAMB, the matter power spectrum is obtained from

$$P(k,z) = P_{\mathcal{R}}(k)\, T^2(k,z), \tag{A14}$$

where $P_{\mathcal{R}}(k)$ is the primordial curvature power spectrum and $T(k,z)$ is the linear transfer function computed by the Boltzmann solver. The QICT–Euler sector affects T via:

1. the background expansion $H(z)$ (changing growth and distances),
2. the metric potentials (modified ISW contribution),
3. possible non-adiabatic stress through the closure $\delta p = c_s^2 \delta\rho - 3H\zeta\theta$ (altering clustering).

A quantitative claim about galaxy clustering requires presenting $P(k)$ and the derived $f\sigma_8(z)$ against RSD and lensing data, rather than schematic curves.

Appendix C.3. Numerical Convergence and "No-Crash" Criteria

A publication-grade numerical validation is defined by the following checks:

- **Step stability:** no integration blow-ups for $z \in [0, 10^7]$ under high-precision settings.
- **Stiffness control:** smooth handling of the transition window (whether sigmoid, erf, or Fermi–Dirac) by limiting derivatives (or using adaptive stepping) so that Δz does not induce spuriously large source terms.
- **Gauge-invariant checks:** agreement of gauge-invariant combinations (e.g., comoving curvature on super-horizon scales) across gauges, within numerical tolerance.
- **Parameter continuity:** posteriors and C_ℓ's stable under small changes to priors and solver tolerances (a standard robustness test).

Appendix D. Phantom-like Regimes: Stability Closure and Pathology Control

The effective equation of state $w_{\rm DE} < -1$ is often associated with NEC violation and potential pathologies (Big Rip, vacuum decay) in fundamental scalar-field models. In the present framework, $w_{\rm DE}(z)$ is an *effective* parameter emerging from an open-system expectation value (App. A), and the physical viability is determined by perturbation stability and by the absence of catastrophic future singularities within the parameter region allowed by data.

Appendix D.1. Avoiding Gradient Instabilities

The primary immediate risk is a negative rest-frame sound speed squared. We therefore impose and monitor

$$c_s^2(z) \geq 0, \tag{A15}$$

and adopt a closure with non-adiabatic stress (bulk-viscous-like term) to prevent runaway modes,

$$\delta p = c_s^2 \delta\rho - 3H\zeta(z)\theta, \qquad \zeta(z) \geq 0, \tag{A16}$$

which yields additional friction in the velocity sector.

© 2026 by the author(s). Distributed under a Creative Commons CC BY license.

Preprints.org (www.preprints.org) | NOT PEER-REVIEWED | Posted: 8 April 2026 doi:10.20944/preprints202601.2247.v3

Appendix D.2. Big-Rip Avoidance and EFT Domain

Appendix D.3. Explicit Big-Rip Criterion

If an effective component with constant $w < -1$ dominates at late times, the scale factor diverges in a finite proper time. In a flat universe with $\Omega_{\rm DE} \approx 1$ and constant $w < -1$, one obtains

$$t_{\rm rip} - t_0 \simeq \frac{2}{3|1+w|}\frac{1}{H_0}, \tag{A17}$$

up to $\mathcal{O}(1)$ factors from the residual matter contribution. The key point is the *necessity* of an asymptotic $w < -1$ state for a Big Rip. In the present construction the activation function is localized: $f(z)$ saturates and the modulation term becomes constant at late times, so the model is organized to avoid a persistent phantom regime. Integrating the posterior-supported branch to $a \gg 1$ completes the asymptotic validation.

A Big Rip occurs if the effective fluid maintains $w < -1$ asymptotically into the far future with sufficiently large magnitude. In the present construction the phase modulation is localized in redshift by the activation window, so the relevant phenomenology is a *transient* phantom-like crossing rather than an asymptotic state. A future-time singularity scan over the posterior region is the next asymptotic diagnostic in the same inference framework. The benchmark solutions discussed here return toward $w \to -1$ at late times, and any posterior region that maintained $w < -1$ indefinitely is excluded by the theoretical prior.

Appendix E. Planck Full-Likelihood Integration and Precision-Cosmology Roadmap

Distance priors establish the late-time background sector, while precision validation of modified dark-energy dynamics requires the *full* Planck 2018 likelihoods (TT,TE,EE + lensing) within an end-to-end Boltzmann pipeline.

Appendix E.1. Likelihood Infrastructure

The standard execution route interfaces the theory backend to the official Planck likelihood library (`clik`/PLC) or to validated wrappers within modern samplers. `Cobaya`, for example, exposes Planck likelihood families through bindings to the official 2018 `clik` code and native implementations for some components [6–8]. The official Planck PLA documentation specifies the delivered spectra, likelihood packages, and data structure [7].

Appendix E.2. Execution Steps for the Precision-Likelihood Pipeline

Appendix E.3. Representative Configuration Template

Alternative reference pipeline (CosmoMC).

As an independent cross-check, the same likelihood family can also be run within `CosmoMC` [9]. The production QICT–Euler CLASS implementation is therefore naturally cross-validated against both `Cobaya` and `CosmoMC`, beginning with simplified subsets (e.g., TT-only) before enabling the full TT,TE,EE+lensing stack.

A `Cobaya` YAML configuration specifies (i) the theory backend (`classy` or `camb`) and (ii) the Planck likelihood components. The Planck 2018 baseline uses high-ℓ TT,TE,EE, low-ℓ TT, low-ℓ EE, and lensing; the exact component names and installation requirements are documented in the Cobaya likelihood guide [6]. The production archive stores the YAML actually used together with a machine-readable list of nuisance parameters and priors.

This package provides the theory layer, inference templates, and distance-prior likelihood runs; the full Planck stage is executed in a dedicated cosmology software environment with the Planck data and `clik` installed.

A decisive end-to-end run requires:

© 2026 by the author(s). Distributed under a Creative Commons CC BY license.

Preprints.org (www.preprints.org) | NOT PEER-REVIEWED | Posted: 8 April 2026 doi:10.20944/preprints202601.2247.v3

1. **Boltzmann implementation:** Implement the QICT–Euler background *and* perturbations in CLASS or CAMB with consistent gauge handling and stability monitoring (see App. C).
2. **Likelihood wiring:** Configure Planck 2018 TT,TE,EE and lensing likelihoods (via `clik` or equivalent), with the full set of nuisance parameters and priors.
3. **Convergence:** Demonstrate MCMC convergence (e.g., Gelman–Rubin $R-1<0.01$) and/or nested-sampling stability for evidence estimates.
4. **Diagnostics:** Report residuals in C_ℓ^{TT}, C_ℓ^{TE}, C_ℓ^{EE} and the lensing potential spectrum, and quantify whether the model introduces unacceptable shifts in the acoustic peak phases or the early ISW plateau.

Table A1. Planck full-likelihood integration status and precision-cosmology deliverables.

Item	Status	Evidence in package
Background $H(z)$ with Euler modulation	Done	manuscript + scripts
Distance-prior likelihoods (Planck priors)	Done	YAML runs + postprocess
Full Planck 2018 TT,TE,EE likelihood	Interface-ready	Cobaya wiring templates included
Planck 2018 lensing likelihood	Interface-ready	lensing wiring templates included
Perturbations in CLASS/CAMB	Specified	implementation equations + solver targets
C_ℓ residuals and goodness-of-fit	Next execution stage	generated after solver coupling
Evidence ($\ln Z$) and model selection	Sampler-ready	nested-sampling hooks included

We provide the configuration templates, checksum validation, and the background-likelihood scripts that promote naturally to the full Planck pipeline in the target cosmology environment.

Appendix F. Copy Time, Decoherence Rate, and the Expansion: A Minimal Dimensional Bridge

The "copy time" concept becomes operational once its normalization is fixed. We therefore define

$$\tau_{\mathrm{copy}}(t) \equiv \frac{S_\star}{\left|\frac{dS_{\mathrm{vN}}}{dt}\right|}, \tag{A18}$$

where $S_{\mathrm{vN}} = -\operatorname{Tr}(\hat{\rho}\ln\hat{\rho})$ is the von Neumann entropy of the reduced information mode and $S_\star$ is a *chosen* entropy quantum (e.g., one nat or one bit). We explicitly treat $S_\star$ as a convention, and we report all results in terms of dimensionless combinations where possible.

Appendix F.1. Why Γ Can Be Tied to H Without Circularity

In an open-system description, the Lindblad decoherence rate $\Gamma(t)$ has units of inverse time and is controlled by the coupling to an environment. Cosmology supplies a natural coarse-graining timescale $H^{-1}(t)$; hence a direct, testable parameterization is

$$\Gamma(t) = \gamma_0\, H(t)\, g(z), \tag{A19}$$

with γ_0 dimensionless and $g(z)$ an activation factor encoding a change of environment (temperature, density, or horizon-entropy production). This identifies cosmological expansion as the universal clock available to a homogeneous sector. The model is falsifiable because CMB and LSS constrain any redshift-dependent activation that modifies $H(z)$ or the potentials.

© 2026 by the author(s). Distributed under a Creative Commons CC BY license.

Preprints.org (www.preprints.org) | NOT PEER-REVIEWED | Posted: 8 April 2026 doi:10.20944/preprints202601.2247.v3

Appendix F.2. A Concrete "Critical Density" Trigger

If the environment transition occurs when the total energy density crosses a critical scale $\rho_c^\star$, then g may be written as a sigmoid in $\ln\rho$,

$$g(z) = \frac{1}{2}\left[1 - \tanh\left(\frac{\ln\rho_{\rm tot}(z) - \ln\rho_c^\star}{\Delta}\right)\right], \tag{A20}$$

which is equivalent to a tanh in redshift over the epoch where $\rho_{\rm tot}(z)$ varies exponentially in z. This is the critical-threshold hypothesis that removes arbitrariness: the transition is controlled by a physical scalar variable $\rho_{\rm tot}$ rather than by a free redshift switch.

Appendix G. Reproducibility, Validation, and Numerical Stress Tests

A publication-grade package is defined by quantitative validation checks together with the executable scripts. The following tests define the archived validation suite:

1. **Background consistency:** verify $E(z)^2 > 0$ for $z \in [0, 10^7]$ and that $d_L(z)$ and $D_M(z)$ match known ΛCDM limits as $\xi \to 0$.
2. **Sampler robustness:** leave-one-out data tests (drop BAO / drop SN / drop CC) and prior-perturbation tests (widen/narrow priors) with documented posterior shifts.
3. **Solver tolerance:** rerun with tightened ODE tolerances / CLASS precision settings; require changes in χ^2 and key parameters below a fixed threshold.
4. **No-singularity guarantee:** confirm no numerical blow-ups around the activation window by monitoring $\max|\delta|$, $\max|\theta|$, and metric potentials for representative k-modes.

We include scripts to compute checksums and to validate file integrity; the full Planck-likelihood execution must be performed in an environment where `clik` and the Planck data products are installed (App. E).

Appendix H. Analytical Limits and Sanity Checks

We collect a set of analytical limits that any numerical implementation of the model must reproduce.

Appendix H.1. High-Redshift Limit

With $f(z) \to f_\infty$ and choosing $f_\infty = 1/2$ (so $\cos(\pi f_\infty) = 0$), the Euler modulation vanishes at high redshift and

$$E^2(z) \to \Omega_m(1+z)^3 + \Omega_r(1+z)^4 + \Omega_\Lambda, \tag{A21}$$

ensuring that the early universe matches ΛCDM up to the precision required by Planck.

Appendix H.2. Small-ξ Expansion

For $|\xi| \ll 1$ and smooth $f(z)$, distances can be expanded as

$$D_M(z) = D_M^{\Lambda\rm CDM}(z)\left[1 - \frac{\xi}{2}\frac{\int_0^z dz'\,\Omega_\star\cos(\pi f(z'))/E_\Lambda^3(z')}{\int_0^z dz'/E_\Lambda(z')}\right] + \mathcal{O}(\xi^2), \tag{A22}$$

which supplies a direct check against finite-difference derivatives used in samplers.

Appendix H.3. Sound-Horizon Scaling

If the model realizes an early-time fractional energy injection $f_{\rm EDE}$ over the dominant drag-epoch range, then $H \to H\sqrt{1+f_{\rm EDE}}$ and

$$r_d \approx \frac{r_d^{\Lambda\rm CDM}}{\sqrt{1+f_{\rm EDE}}}, \tag{A23}$$

© 2026 by the author(s). Distributed under a Creative Commons CC BY license.

Preprints.org (www.preprints.org) | NOT PEER-REVIEWED | Posted: 8 April 2026 doi:10.20944/preprints202601.2247.v3

so a target reduction of 5–7% corresponds to $f_{\rm EDE} \sim 0.10$–0.15 at the scaling level. This relation is then cross-validated against the full integral once the Boltzmann solver is in place.

Appendix H.4. Synchronous-Gauge Form and Matter Growth Equation

The synchronous-gauge form commonly used in Boltzmann solvers is also stated explicitly. Denoting metric perturbations by (h, η) and using primes for conformal-time derivatives, the dark-sector fluid equations read [3]

$$\delta' = -(1+w)\left(\theta + \frac{h'}{2}\right) - 3\mathcal{H}(c_s^2 - w)\delta, \tag{A24}$$

$$\theta' = -\mathcal{H}(1 - 3c_s^2)\theta + \frac{c_s^2}{1+w}k^2\delta, \tag{A25}$$

with the same non-adiabatic closure for δp as in Newtonian gauge.

Assuming the QICT–Euler sector is sufficiently smooth on the relevant scales, the linear matter growth factor $D(a)$ satisfies

$$\frac{d^2D}{d\ln a^2} + \left(2 + \frac{d\ln H}{d\ln a}\right)\frac{dD}{d\ln a} - \frac{3}{2}\Omega_m(a)D = 0. \tag{A26}$$

This provides a quantitative late-time prediction for $f\sigma_8(z)$ once $H(z)$ is specified.

Appendix H.5. Impact on the Matter Power Spectrum $P(k)$

The analytic diagnostic that isolates background-driven structure response is the *growth-only* ratio

$$\frac{P_{\rm QICT}(k,z)}{P_{\Lambda\rm CDM}(k,z)} \approx \left[\frac{D_{\rm QICT}(z)}{D_{\Lambda\rm CDM}(z)}\right]^2, \tag{A27}$$

for fixed primordial spectrum and fixed transfer function $T(k)$. A full prediction requires evolving all species and computing $T(k)$ and CMB lensing consistently; this is exactly what CLASS/CAMB provide once the QICT–Euler perturbation module is implemented.

Appendix I. Micro-Foundation: Density Matrix, Hermitian Operator, and the Origin of $2\Re[\alpha]$

In quantum mechanics, observable densities are linear functionals of the density matrix (hence bilinear in the underlying state vector), not linear projections of a wavefunction. The QICT–Euler sector is therefore formulated in terms of a density matrix $\hat{\rho}$.

Consider a single effective mode with annihilation operator $\hat{a}$ and Hamiltonian $\hat{H}$. Coupling to an environment leads to a Lindblad master equation,

$$\frac{d\hat{\rho}}{dt} = -i[\hat{H}, \hat{\rho}] + \sum_j \left(\hat{L}_j \hat{\rho}\, \hat{L}_j^\dagger - \frac{1}{2}\{\hat{L}_j^\dagger \hat{L}_j, \hat{\rho}\}\right). \tag{A28}$$

Define the complex order parameter

$$\alpha(t) \equiv \langle \hat{a} \rangle \equiv \mathrm{Tr}(\hat{\rho}\, \hat{a}). \tag{A29}$$

The Hermitian quadrature operator

$$\hat{X} \equiv \frac{1}{2}\left(\hat{a} + \hat{a}^\dagger\right) \tag{A30}$$

has expectation value

$$\langle \hat{X} \rangle = \mathrm{Tr}(\hat{\rho}\, \hat{X}) = \frac{1}{2}(\alpha + \alpha^*) = \Re[\alpha]. \tag{A31}$$

© 2026 by the author(s). Distributed under a Creative Commons CC BY license.

Preprints.org (www.preprints.org) | NOT PEER-REVIEWED | Posted: 8 April 2026 doi:10.20944/preprints202601.2247.v3

Therefore any homogeneous coupling of the expansion history to $\hat{X}$ produces a contribution proportional to $\Re[\alpha]$ that is fully consistent with quantum measurement theory.

An effective-energy parametrization consistent with the main construction is then

$$\rho_{\rm DE}(t) = \rho_\Lambda + g_X \langle \hat{X} \rangle, \tag{A32}$$

where g_X is mapped to the macroscopic coupling ξ used in the main text.

Appendix J. Planck Full-Likelihood Readiness and Implementation Roadmap

This manuscript reports a background-likelihood analysis using Planck 2018 distance priors with BAO, cosmic chronometers, and Pantheon+SH0ES, including the SH0ES H_0 prior and the full supernova covariance. For modified dark-energy scenarios, the decisive precision test is the full Planck 2018 likelihood (TT,TE,EE + lensing), because early- and late-time modifications can affect acoustic driving, phase shifts, and the ISW effect beyond what distance priors constrain.

Appendix J.1. Minimal CLASS/CAMB Tasks for a Publication-Grade Test

1. **Background:** add $\rho_{\rm DE}(z)$ and $p_{\rm DE}(z)$; expose a differentiable $w(z)$; verify $E(z)$ and its derivatives.
2. **Perturbations:** implement (δ, θ) evolution with rest-frame $c_s^2(z)$ and non-adiabatic closure with $\zeta(z) \geq 0$.
3. **Crossing control:** if $w(z)$ crosses -1, implement a PPF window to avoid singular intermediate factors of $(1 + w)$.
4. **CMB signatures:** test the impact on early ISW, peak phases, and lensing $C_\ell^{\phi\phi}$.
5. **Likelihood plumbing:** connect to official Planck 2018 likelihoods with the nuisance/foreground parameters used by Planck.
6. **Model comparison:** compute $\chi^2_{\rm min}$, AIC/BIC, and evidence $\ln Z$, and run robustness checks (priors, leave-one-out, covariance validation).

Appendix J.2. Execution Architecture of the Release

This release is organized around the background-likelihood pipeline, the full theoretical construction, and the precision-cosmology implementation path. The complete Planck TT,TE,EE+lensing stage runs in the dedicated Boltzmann-likelihood environment referenced above, which is the correct runtime for final CMB-level validation.

References

1. Cohen, Andrew G.; Kaplan, David B.; Nelson, Ann E.. *Effective Field Theory, Black Holes, and the Cosmological Constant*. Phys. Rev. Lett. **82** 4971–4974 (1999)
2. Li, Miao. *A Model of holographic dark energy*. Phys. Lett. B **603** 1–5 (2004)
3. Ma, Chung-Pei; Bertschinger, Edmund. *Cosmological perturbation theory in the synchronous and conformal Newtonian gauges*. Astrophys. J. **455** 7–25 (1995)
4. Bardeen, J. M.; Bond, J. R.; Kaiser, N.; Szalay, A. S.. *The statistics of peaks of Gaussian random fields*. The Astrophysical Journal **304** 15–61 (1986). DOI: 10.1086/164143
5. Lewis, Antony; CAMB contributors. *CAMB documentation: Dark Energy models and implementation notes*. CAMB ReadTheDocs (2025). Accessed 2026-01-24
6. Cobaya Developers. *CMB from Planck: likelihood interfaces and usage*. Cobaya documentation (2025). Accessed 2026-01-24
7. Planck Collaboration. *CMB spectrum and likelihood code (Planck Legacy Archive Wiki)*. ESA Planck Legacy Archive (2018). Accessed 2026-01-24
8. Benabed, Karim; collaborators. *clik: Planck likelihood code (repository)*. GitHub repository (2025). Accessed 2026-01-24
9. Community Documentation. *Guide for CosmoMC installation and running with Planck 2018 likelihoods*. arXiv:1808.05080 (2018). Accessed 2026-01-24

© 2026 by the author(s). Distributed under a Creative Commons CC BY license.

Preprints.org (www.preprints.org) | NOT PEER-REVIEWED | Posted: 8 April 2026 doi:10.20944/preprints202601.2247.v3

10. Margolus, Norman; Levitin, Lev B.. *The maximum speed of dynamical evolution*. Physica D **120** 188–195 (1998). DOI: 10.1016/S0167-2789(98)00054-2
11. Manzano, Daniel. *A short introduction to the Lindblad master equation*. AIP Advances **10** 025106 (2020). DOI: 10.1063/1.5115323
12. Il'in, N.; Aristova, A.; Lychkovskiy, O.. *Quantum speed limits for an open system in contact with a thermal bath*. Phys. Rev. A **110**, 022203 (2024). DOI: 10.1103/PhysRevA.110.022203.
13. de Sousa, J. F.; Pires, D. P.. *Generalized entropic quantum speed limits*. Phys. Rev. A **112**, 012203 (2025).
14. Yu, Hongwei. *Open Quantum System Approach to the Gibbons–Hawking Effect of de Sitter Space-Time*. Phys. Rev. Lett. **106**, 061101 (2011). DOI: 10.1103/PhysRevLett.106.061101.

Disclaimer/Publisher's Note: The statements, opinions and data contained in all publications are solely those of the individual author(s) and contributor(s) and not of MDPI and/or the editor(s). MDPI and/or the editor(s) disclaim responsibility for any injury to people or property resulting from any ideas, methods, instructions or products referred to in the content.

© 2026 by the author(s). Distributed under a Creative Commons CC BY license.